BUILD SIMUL (2017) 10: 769–781
DOI 10.1007/s12273-017-0352-5

Multi-objective optimization of HVAC system using NSPSO and Kriging algorithms—A case study

Nan Li[1], Sherman C.P. Cheung[1] (✉), Xiaodong Li[2], Jiyuan Tu[1]

1. School of Engineering, RMIT University, Australia
2. School of Science, RMIT University, Australia

Abstract

In modern building design, engineers are constantly facing challenging to find an optimal design to maintain a high level of thermal comfort and indoor air quality for occupants while minimizing the system energy consumption. Over the past decades, several algorithms have been proposed and developed for optimizing the heating, ventilation and air conditioning (HVAC) system for indoor environment. Nevertheless, majority of these optimization algorithms are focused on single objective optimization procedures and require large training sample for surrogate modelling. For multi-objective HVAC design problems, previous studies introduced an arbitrary weighting factor to combine all design objectives into one single objective function. The near optimal solutions were however sensitive to the chosen value of the weighting factor. Aiming to develop a multi-objective optimization platform with minimal computational cost, this paper presents a nondominated sorting-based particle swarm optimization (NSPSO) algorithm together with the Kriging method to perform optimization for the HVAC system design of a typical office room. In addition, an adaptive sampling procedure is also proposed to enable the optimization platform to adjust the sampling point and resolution in constructing the training sample. Significant computational cost could be reduced without sacrificing the accuracy of the optimal solution. The proposed methods are applied and assessed in a typical HVAC system and the results indicate that comparing to traditional methods, the presented approach can handle multi-objective optimization in ventilation system with up to 46.6% saving of computational time.

Keywords

multi-objective optimization,
CFD,
NSPSO,
Kriging surrogate,
adaptive sampling

Article History

Received: 25 September 2016
Revised: 12 January 2017
Accepted: 24 January 2017

1 Introduction

In the modern indoor environment design, driven by the higher expectation of occupants and soaring energy cost, indoor thermal comfort and energy efficiency are the two main concerns in the heating, ventilation and air conditioning (HVAC) systems. To achieve a higher system performance, computational fluid dynamics (CFD) simulation tools such as ANSYS Fluent, StarCCM+ and OpenFOAM have been widely adopted to analyze air distribution and flow characteristics and their relationship in thermal comfort and energy consumption (Ravikumar and Prakash 2009; Cardinale et al. 2010; Hiyama et al. 2010; Kochetov et al. 2015; Gangisetti et al. 2016).

In comparison to the traditional design cycle, CFD simulations offer a faster and more economical way for engineers to carry out parametric studies, leading towards a more desirable system design. According to our previous works (Tu et al. 2008), CFD has been proved to be a reliable prediction tool which has been widely adopted in industrial applications and academia research. Albeit a near-optimum solution could be obtained, the parametric analysis using CFD technique is inherently discrete in the design space with pre-selected design variable values. The best optimum solution could be "hidden" in the discretized domain (Stavrakakis et al. 2011). Furthermore, the accuracy of a near-optimum solution depends largely on the "resolution" of the test matrix where significant computational costs are required. To enhance the accuracy of the near-optimum solution with practical computational time and resource,

E-mail: chipok.cheung@rmit.edu.au

artificial neural network (ANN) (Varol et al. 2007; Zhou and Haghighat 2009a,b; Stavrakakis et al. 2011; He et al. 2014) or other surrogate techniques (Li et al. 2013a,b) are employed as an alternative approach to approximate the nonlinearity and complex behaviour of the multidimensional systems. One of the first studies using CFD-ANN coupled approach to assess the effect of architectural-designs on the thermal comfort can be found in (Krauss et al. 1997). In general, numerical results predicted by CFD modelling were adopted to establish a database for training the ANN or surrogate models. These CFD-trained ANN or surrogate models then captured the relationship between design parameters and objective function. Optimization procedures using gradient methods (Gyulai et al. 2007; Stavrakakis et al. 2011; Welle et al. 2011) or evolutionary optimization algorithms (Luh and Lin 2011; Li et al. 2013b; Afrand et al. 2015; Zhai et al. 2014) were then performed using the trained models for allocating the near-optimum solution within the continuous design space. Although significant computational time and resource can be reduced, a considerably large amount of CFD results are still required for constructing a reliable database for the training of ANN or surrogate models.

On the other hand, most of the HVAC system design normally involves multi-objective considerations. Design indices such as predicted mean vote (PMV), percentage dissatisfied of draft (PD), age of air, CO_2 concentration and energy cost are commonly considered in literature. Especially, in terms of indoor thermal comfort evaluation, substantial research works have done by Ricciardi's group (Buratti and Ricciardi 2009; Buratti et al. 2013, 2016; Nematchoua et al. 2014; Ricciardi and Buratti 2015; Ricciardi et al. 2016). In most previous works, a single objective function was constructed by aggregating several design indices using pre-defined weighting factors (Laverge and Janssens 2013; Li et al. 2013b). One particular disadvantages of this method is that the optimal solution could be sensitive to the values of the weighting factors. In other words, different values of weighting factors could result in substantially different solutions. The weighting factors must be therefore chosen carefully based on subjective factors such as engineering or expert judgements. Furthermore, the optimization procedure gives only one near optimal solution where there is no flexibility for the designer to strike a balance or "trade-off" of the conflicting parameters. For example, a lower indoor temperature may be preferable in summer which is in conflict with the goal to minimize energy consumption.

As an attempt to overcome the aforementioned shortcoming, in this study, we propose the use of a nondominated sorting-based particle swarm optimization (NSPSO) algorithm to achieve multi-objective optimization without having to use any weighting factors. This population-based algorithm, as an improved technique of the basic particle swarm optimization (PSO), is capable to obtain a set of nondominated solutions (i.e. approximated Pareto Front solutions); providing the engineers a set of optimal solutions where the most appropriate design solution based on professional judgment or end-user desire can be chosen (Carrese et al. 2011). Furthermore, to minimize the computational requirement for constructing a reliable training database, Kriging or Gaussian process regression together with adaptive sampling technique is also adopted to dynamically allocate additional CFD simulation dataset where there is a higher likelihood of having a near optimal solution. A case study is used to demonstrate the feasibility of the proposed optimization approach in a real-world HVAC application.

2 Multi-objective optimization methods

2.1 Basic principles of particle swarm optimization

Traditional mathematical programming methods for solving both single- and multi-objective optimization problems have been successfully adopted in many science and engineering problems (Martínez 2013). Nevertheless, it is also well known that these methods have difficulty in solving non-convex and multimodal problems (Deb 2001). In contrast, population-based stochastic optimization methods such as evolutionary algorithms (EAs) have the advantage of not requiring gradient information in the optimization process which could provide remedy for this class of problems (Martínez 2013). Among existing population-based stochastic optimization methods, particle swarm optimization (PSO) has proven to be faster in convergence in comparison with standard EAs (Hassan et al. 2005). PSO was first introduced by Kennedy (2001) based on the inspiration drawn from observations of the social behaviours of insects including learning from previous experience and communicating with successful individuals. In PSO, each particle has its own position and velocity, which are represented by x_i and v_i, respectively. The position and velocity of the particle are updated according to the following equations:

$$\begin{aligned} v_i(\mathrm{t}+1) &= \omega v_i(\mathrm{t}) + c_1\varphi_1(p_i - x_i(\mathrm{t})) + c_2\varphi_2(p_\mathrm{g} - x_i(\mathrm{t})) \\ x_i(\mathrm{t}+1) &= x_i(\mathrm{t}) + v_i(\mathrm{t}+1) \end{aligned} \quad (1)$$

where p_i and p_g represent the personal best position and global best position, respectively, and the c_1 and c_2 are two uniform random numbers within the range [0, 1]. The φ_1 and φ_2 are two constants which are usually set to 2. The parameter ω decreases with iterations within the range [0.4, 1.2]. To avoid going out of the search space, both the position and velocity are limited within boundaries, $[x_{\min}, x_{\max}]$ and

$[v_{min}, v_{max}]$, respectively. Nevertheless, it is worth noting that the original PSO can only provide solutions for single-objective optimization problems.

2.2 Nondominated sorting-based PSO

Inspired by the works done by Deb et al. (2002), Li (2003) proposed a Nondominated Sorting Method to extend the original PSO to multi-objective optimization problems (MOP)—namely nondominated sorting-based particle swarm optimization (NSPSO). In NSPSO, the updating equations for particle position and velocity remain unchanged, but the selection of the personal best and global best has been re-designed. Two main mechanisms are used to determine the global best among the population — (1) nondominated sorting for identifying different fronts, and (2) crowding distance computed for particles within each front to encourage solution diversity. These kinds of information are used to select suitable leaders (i.e. global best) at each iteration to guide the particles moving towards the Pareto-optimal Front while still maintaining a good distribution of solutions along the Pareto Front.

2.2.1 *Nondominated Sorting*

Figure 1 shows an example of the nondominated sorting process. Considering 2 objectives (i.e. f_1 and f_2) to be optimized in the process, the entire population (i.e. the 10 particles that labelled as 1 to 10) is sorted into different levels of fronts according to the domination comparisons between particles. The particles in same front are nondominated with each other. As depicted in Fig. 1, Front 1 is the highest-level nondominated front because all particles in it are not dominated by any other particles in the entire population. The main goal of nondominated sorting is to classify the whole population into different levels of nondominated fronts. The global best particle (leader of the population) can be randomly selected from the highest-level front. This kind of selection process will push the whole population towards the true Pareto Front. More information regarding nondominated sorting can be found in (Li 2003).

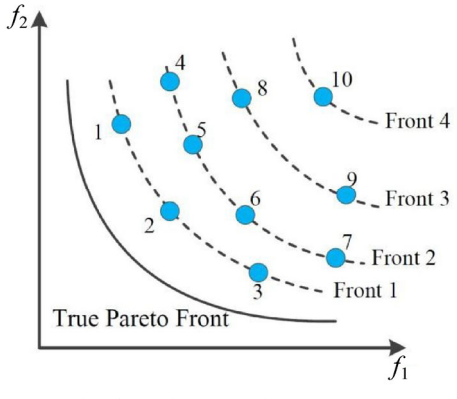

Fig. 1 An example of nondominated sorting process in NSPSO

2.2.2 *Crowding distance*

Unlike in single-objective optimization, maintaining the diversity in a set of solutions is vital in a multi-objective optimization (Deb et al. 2002; Li 2003). Throughout the optimization process, the leader must be selected properly to avoid local optimal aggregation of the whole population. In NSPSO, computing the crowding distance values among particles in the highest-level of nondominated front is used to select leaders that are both good and far apart from each other. Inspired by (Deb et al. 2002), we introduced a new way to calculate the crowding distance. Figure 2 shows an example of the crowding distance among particles. For each particle, the crowding distance is defined as the following:

$$D_n = \begin{cases} \infty & n = 1, N \\ d_{n-1} + d_n & 1 < n < N \end{cases} \quad (2)$$

The particle with a higher crowding distance value will have a high probability to be selected as the leader. Consequently, particles in the top front are likely to maintain a good level of population diversity.

2.3 Surrogate modelling

Evolutionary optimization algorithms are efficient in obtaining a representation of the Pareto Front for the MOP (Carrese et al. 2011). However, generating all the elements in an objective array by simulations could still be computationally demanding. Previous studies have adopted surrogate modelling techniques (e.g. ANN (Varol et al. 2007; He et al. 2014) and support vector machine (SVM) (Zhao 2009)) which is trained by computational simulated samples to achieve substantial saving in computational time and resources. However, to ensure its accuracy, ANN and SVM

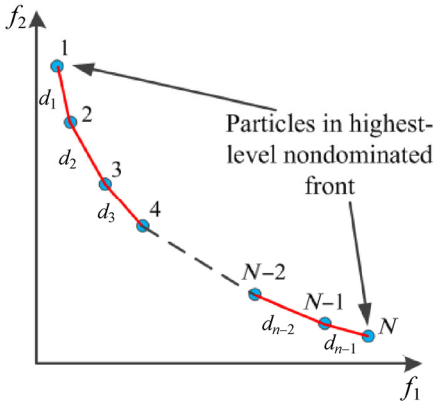

Fig. 2 Crowding distances among individuals in the highest-level nondominated front

require considerably large training samples which pose significant burden on the computational cost. Alternatively, other than the ANN and SVM algorithms, the Kriging method has aroused much attention due to its capability in achieving high prediction accuracy with relatively small training sample size. Aiming to minimize the computational cost for large training samples, Kriging method is therefore adopted and incorporated with NSPSO in the present study. A brief introduction to the Kriging method is presented in this section. More detailed derivation and formulation of the Kriging method can be found in (Forrester et al. 2008) and the references therein. The Kriging technique provides the best linear unbiased estimator of the unobserved fields based on the sampled data (Journel and Huijbregts 1978). The basic idea of Kriging is to predict the value of a function at a given point by computing a weighted average of the known values of the function in the neighborhood of the point, which is expressed as

$$\hat{z}(\mathbf{x}_L) = \sum_{\alpha=1}^{N} \lambda_\alpha z(\mathbf{x}_\alpha) \tag{3}$$

where $\hat{z}(\mathbf{x}_L)$ represents a local estimation at the data location $\mathbf{x}_L$, $z(\mathbf{x}_\alpha)$ is the sampled value at the data location $\mathbf{x}_\alpha$ and λ_α represents the weighting coefficient which can be calculated by minimizing the estimation variance:

$$\min E\left\{\left[z(\mathbf{x}_L) - \hat{z}(\mathbf{x}_L)\right]^2\right\} = C(0) - 2\sum_{\alpha} \lambda_\alpha C(\|\mathbf{x}_\alpha - \mathbf{x}_L\|) + \sum_{\alpha}\sum_{\beta} \lambda_\alpha \lambda_\beta C(\|\mathbf{x}_\alpha - \mathbf{x}_\beta\|) \tag{4}$$

subjects to the unbiased condition:

$$E[z(\mathbf{x}_L) - \hat{z}(\mathbf{x}_L)] = 0 \tag{5}$$

and the normalization condition:

$$\sum_{\alpha=1}^{N} \lambda_\alpha = 1 \tag{6}$$

The weighting coefficient λ_α in Eq. (3) can be solved using a quasi-Newton optimization method or other similar algorithm (Gano et al. 2006). Finally, the prediction value at the unobserved location can be given by Eq. (3).

3 Case description

3.1 CFD modelling and validation

To assess the feasibility and performance of the aforementioned approach, this investigation focuses on a practical HVAC design optimization case study where the air quality, thermal comfort and energy consumption of a typical office room are optimized against the supply air velocity and supply air temperature (Zhou and Haghighat 2009a; Li et al. 2013b). The case study is constructed with a reference to a full-scale experimental measurements reported by Yuan et al. (1999). Figure 3 shows a three-dimensional representation of the typical office room. According to the experimental setup, the outside temperature is 26.7 °C, and room temperature is maintained between 23.3 °C and 26 °C using displacement ventilation system. The supply cooled air is discharged one side at the low level of the room (i.e. label 1 in the figure) and the return air leaves the room from the exhaust at the center of the ceiling (i.e. label 2). Two heat sources mincing two office workers were placed in the room (i.e. labels 3 and 4). Computers and lightings were also dissipating heat to the room. In this study, all simulations are assumed to be steady state where ideal gas law was adopted for the air properties. More details of boundary conditions have been tabulated in Table 1. Based on the previous work by Yuan et al. (1999), experimental measurements were carried out within an environmental chamber where solar radiation contribution was neglected. To validate our CFD with the experimental data, no solar radiation is incorporated in the simulation.

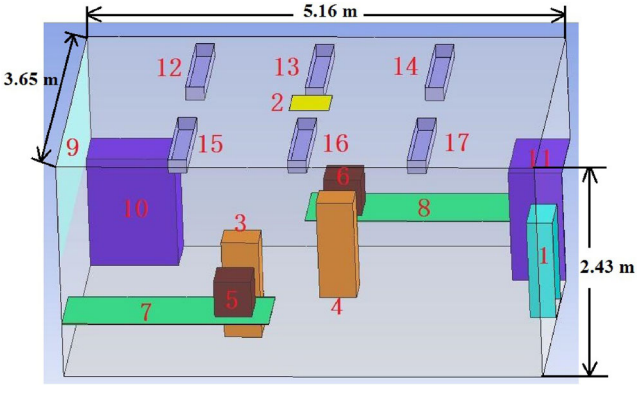

Fig. 3 The geometry layout of the typical office room

Table 1 The boundary conditions adopted in the CFD simulations

Number	Name	Boundary details	Comments
1	Air-conditioning	Normal speed & static temperature	Controlled variables
2	Exhaust	Average static pressure	0 Pa
3,4	Occupant	Temperature	37 °C
5,6	Desktop	Heat flux	108.5 W/m^2
7,8	Table	Adiabatic	—
9	Partition window	Heat transfer coefficient	3.7 W/(m^2·K)
10,11	Furniture	Adiabatic	—
12–17	Light	Heat flux	34 W/m^2
	Room wall	Heat transfer coefficient	0.19 W/(m^2·K)

A CFD model of the office room was built in ANSYS Workbench, which contains in total 1,043,811 nodes and 2,849,852 elements. To ensure the validity of the CFD simulation, predictions of the CFD model were first validated against the full-scale experimental data reported by Yuan et al. (1999). In the experiment, a hot-sphere anemometer system was used for air velocity, velocity fluctuation measurements and a thermocouple system was used to measure surface and air temperatures. Figure 4 shows the comparisons between the measured and predicted air temperature and velocity along the vertical line at the center of the office room where supply air temperature and velocity were maintained at 17 °C and 0.09 m/s respectively.

As depicted, the predicted temperature variation was successfully captured by the CFD model and compared well agreed with the measurements. Similarly, the velocity profile was also in good agreement with the experiment. These encouraging results show the reliability of the CFD predictions and its capability for providing sampling data for the design optimization procedures.

3.2 Optimization objectives

In the presented study, the predicted mean vote, CO_2 concentration, and energy consumption were adopted to quantitatively assess the performance of the HVAC system in terms of thermal comfort, air quality and energy efficiency respectively. The definition of the predicted mean vote, CO_2 concentration, and energy consumption are briefly discussed in the following sections.

3.2.1 *Predicted mean vote*

The predicted mean vote (PMV) is a thermal comfort evaluation index which was first introduced by Fanger (1972). It is used to assess indoor thermal comfort based on heat balance and a set of experimental data collected from a given controlled climate chamber. The index represents the mean subjective satisfaction with the indoor thermal environment with a number between −3 (cold) and +3 (hot). The zero value is defined as the ideal representation of thermal neutrality. The PMV index is evaluated based on an empirical equation which is correlated to the local air temperature, mean radiant temperature, relative humidity, air speed, metabolic rate, and clothing insulation (Fanger 1972). In this study, we assume that the occupants are seated in quiet position (i.e. metabolic rate of 1.0 met) with a summer clothing (i.e. 0.2 clo), and we evaluated the average PMV based on the predicted field information obtained from CFD simulations.

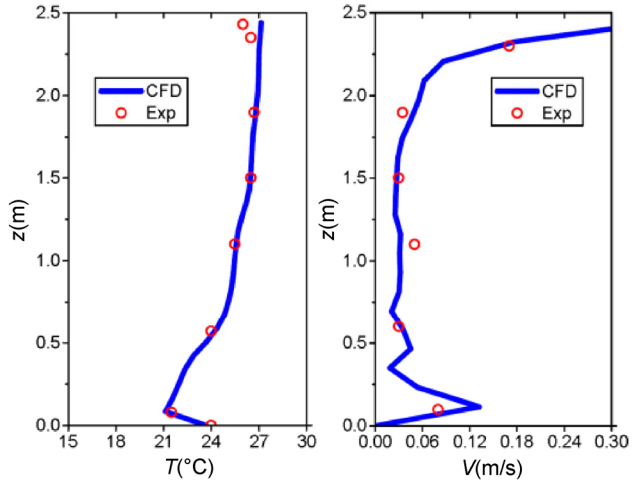

Fig. 4 Comparisons between the CFD simulation results and experimental data

3.2.2 *CO_2 concentration*

To assess the air quality within the space, the concentration of CO_2 emitted by occupants throughout the office room was also resolved in the CFD simulation. In the simulation, the CO_2 is emitted from the occupants with the emission rate 0.87 L/min. Similar to the average PMV, the average CO_2 concentration was extracted from the predicted CFD field information.

3.2.3 *Energy consumption*

Following the previous study (Zhou and Haghighat 2009a; Li et al. 2013b), the energy consumption of the air-conditioning system is divided into two parts: ventilation fan power and the cooling or heating load. Energy consumption in the two parts is determined as follows:

$$E_{\text{fan}} = \frac{P \cdot V_{\text{air}}}{\eta_{\text{fan}}}$$
$$E_{\text{cooling/heating}} = m_{\text{supply}} c_{\text{p}} (T_{\text{return}} - T_{\text{supply}}) + m_{\text{outdoor}} (h_{\text{outdoor}} - h_{\text{return}})$$
$$E_{\text{total}} = E_{\text{fan}} + E_{\text{cooling/heating}} \quad (7)$$

where P is the air pressure difference of the fan, η_{fan} is the fan efficiency which is assumed to be 0.75, V is the volume flow rate of supply air (m^3/s), m represents the mass flow rate of the air (kg/s), c_p is the specific heat capacity of air, T represents the temperature, h is the specific enthalpy of air (J/kg) which is related to air temperature and relative humidity. Similarly, we can get energy costs from the CFD-Post package.

4 Optimization results and analysis

4.1 Multi-objective optimization platform

As mentioned earlier, the aim of this case study is to optimize the value of |PMV|, CO_2 concentration and energy

consumption against a set of control design parameters (i.e. supply air velocity and temperature). However, these three indices are in conflict with each other, which means there does not exist an optimal solution where all indices are at the minimal value. Weighting factors were used to get trade-off solutions in previous research (Zhou and Haghighat 2009a; Li et al. 2013b). In order to overcome the drawbacks of the weighting methods, we proposed a multi-objective optimization platform by integrating the CFD modelling technique, Kriging method and NSPSO algorithm to consider the three objectives simultaneously and obtain the corresponding Pareto Front of without any weighting factor. A schematic of the methodology is depicted in Fig. 5.

As depicted in the flowchart, the CFD simulation technique is adopted to establish the sample data as the input of the Kriging method. Following the previous studies (Zhou and Haghighat 2009a; Li et al. 2013b), a total of 25 CFD simulations with different combinations of controlled variables have been carried out (see also Fig. 6). Similar to the validation study, all simulations were carried out using the ANSYS CFX 14.5 with the identical mesh resolution and boundary conditions (except the supply air temperature and velocity). Based on the simulated results, local air velocity, temperature and associated parameters were extracted for evaluating the corresponding PMV, CO_2 concentration and energy consumption value. All the obtained values (i.e. a total of 25 set of data) were then used to construct the sample data for the Kriging method. In terms of thermal comfort, we would like the PMV value to be as close to 0 as possible. At the same time, we also would like to minimize CO_2 concentration and energy consumption. In order to describe the conflicting relationships among these three objectives, we listed three groups of typical values in Table 2. The first row in Table 2 shows the point where the PMV is the closest to 0 while both the CO_2 concentration and the energy consumption are quite large. Similarly, the second and the third rows show the points where the CO_2 concentration and the energy consumption are minimum, respectively, while the other two objectives are quite large. Therefore, these three objectives are conflicting with each other. We cannot find a point where all the objectives are at their minimum value. As we mentioned before, traditional methods using weighting factors for solving MOP are inefficient. In this paper we developed a multi-objective optimization platform based on NSPSO to solve MOP efficiently. The details and results will be described in the following.

In order to study the accuracy of the Kriging prediction, 16 more CFD simulations were added, which are located in the center of each sampling grid. We compared the values of the three objectives exported from the CFD-Post with the values predicted by the fully Kriging surrogate model (i.e. the Kriging model using all the 25 CFD sample data defined in Fig. 6). The percentage errors between the CFD results and the Kriging prediction are shown in Fig. 7. From Fig. 7, we can see that the maximum errors of prediction for PMV and CO_2 are less than 5.2% and the maximum error of prediction for energy is less than 0.6%, which indicates the Kriging prediction has achieved a good accuracy.

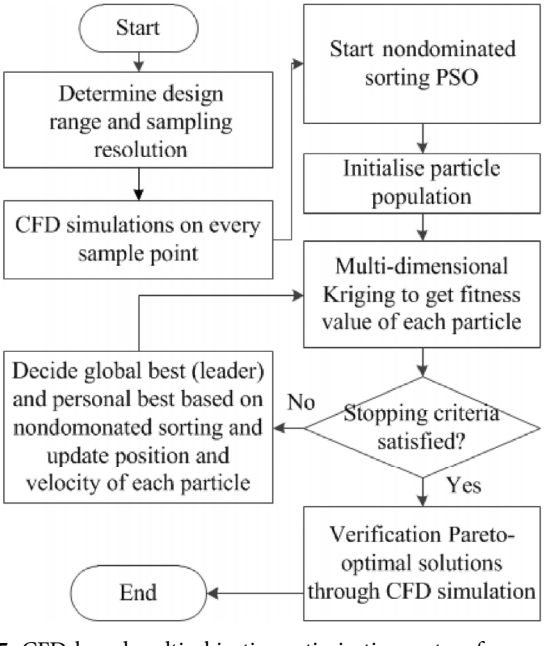

Fig. 5 CFD-based multi-objective optimization system framework

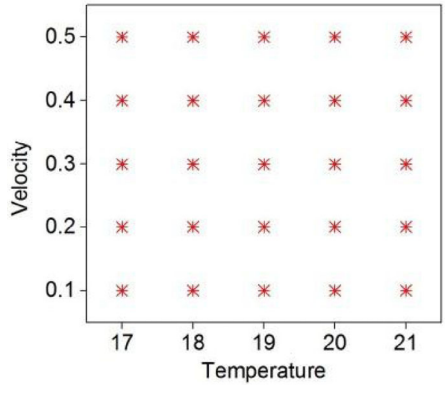

Fig. 6 Definitions of inlet boundary conditions in CFD simulations

Table 2 Three typical groups of values minimizing PMV, CO_2, energy, respectively

T (°C)	V (m/s)	PMV	CO_2 (mg/L)	Energy (W)
19.5	0.19	−0.063	0.078	863.6
21	0.5	−0.964	0.028	1671.8
21	0.1	0.327	0.083	334.4

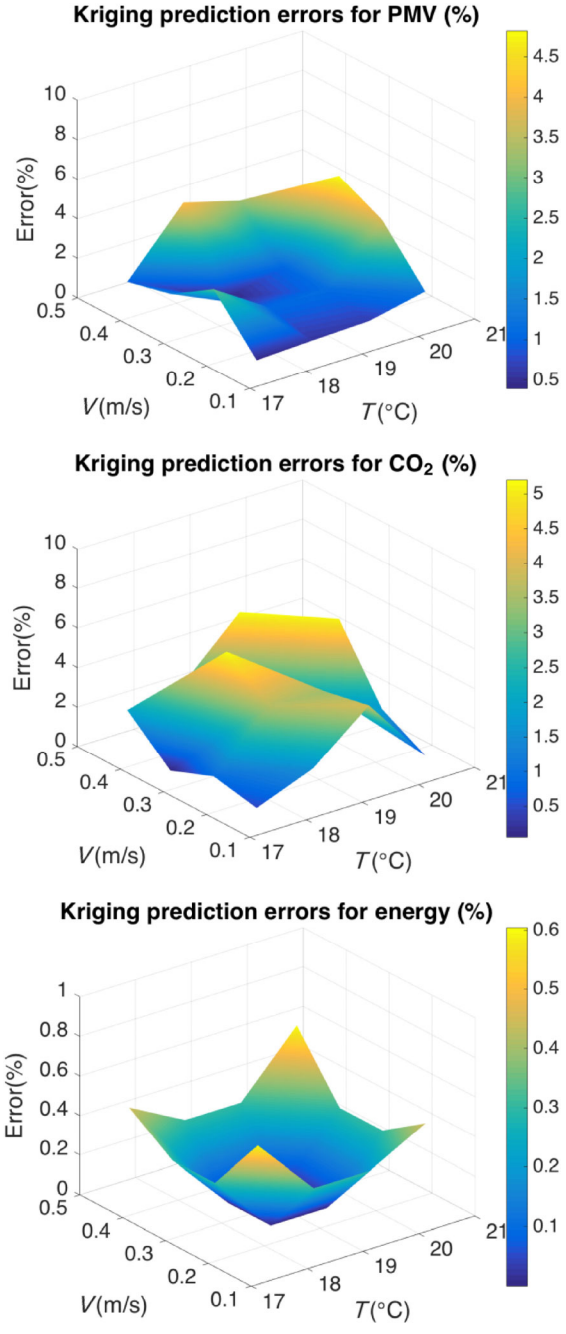

Fig. 7 Percentage errors of Kriging prediction for the three objectives—PMV, CO_2 and energy, respectively

Afterward, a three-objective optimizer based on the NSPSO algorithm was implemented using the MATLAB R2013b. In the optimization procedure, the Kriging surrogate method was used to calculate the fitness values for each particle in the population. The initial size of the swarm population was 200 and the maximum iteration number was set to be 100. Figure 8 shows the trade-off solutions given by the NSPSO algorithm. The blue dots represent the finally reserved particles in the objective space, which constitute a set of solutions approximating the Pareto Front.

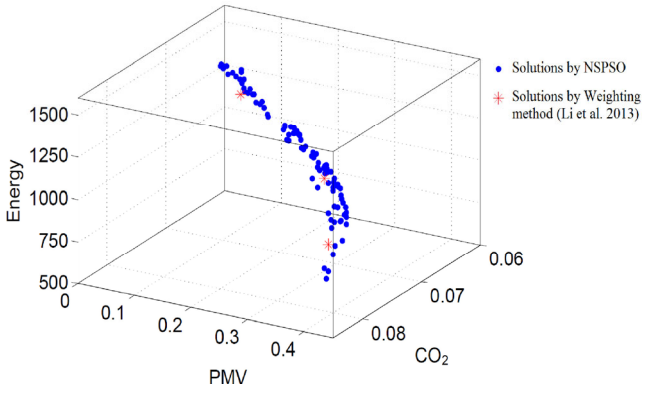

Fig. 8 Comparison of solutions given by NSPSO and solutions given by Weighting method in 3D objective space

In order to compare our results with the results given by weighted method introduced in (Li et al. 2013b), the previous results are also plotted in Fig. 8 (shown as red stars). Each red star in Fig. 8 represents a solution given by a set of fixed weighting factors. From the comparison, we can notice that the solutions given by previous method (red stars) are only a small subset of the Pareto Front given by our approach. It is also noted that our approach does not depend on any weighting factor, and after only one simulation run, a set of trade-off solutions can be found in the objective space, providing the designers with the choices of a range of trade-off solutions.

4.2 Adaptive sampling for Kriging

The above section has clearly demonstrated the capacity of the proposed multi-objective optimization platform. By replacing the CFD simulations with the Kriging method, the optimization process could reduce significantly the computational time. Nevertheless, in constructing the sample data, CFD simulations are uniformly distributed within the design range (see Fig. 6). The main disadvantage of uniform sampling is its high cost, because the sampling density must be uniformly high everywhere in order to meet the sampling requirements in some particular area. Nevertheless, in most practical cases, the final optimal solutions are normally concentrated in a certain region within the design space. Therefore, substantial computational time could be wasted in constructing the sample data for some virtually redundant samples which are far away from the optimal solution. To strike a balance between accuracy and computational cost, the sampling points should be strategically placed in the region where has a higher likelihood of getting optimal solutions rather than uniformly distributed throughout the design space. To achieve this, we introduced an adaptive sampling procedure to determine sampling point. Adaptive sampling designs, also known as response-

adaptive designs, are ones where the accruing data (i.e., the observations) are used to adjust the experiment as it is being run (Hardwick and Stout 2016). The adaptive sampling method is then adopted to govern the construction of the sample data where sampling points are allocated based on the likelihood of having optimal solution within the region. A flowchart showing the procedures in constructing the sample data for Kriging and its integration with the multi-objective optimization platform is also shown in Fig. 9.

To assess the potential computational saving, the adaptive sampling procedure will be applied to the same HVAC design optimization case study and compared against the results from uniform sample data (i.e. as presented in previous section). To make a comparison with the previous result, instead of locating the sampling point in any point within the design space, the adaptive sampling method is applied to determine the next sampling location based on halving method. This is to ensure the sampling locations are consistent with the uniform sampling method. To initialize the process, four sampling locations (red stars in Fig. 13) were firstly specified at all corners of the design space (i.e. corner at the minimum and the maximum value of supply air temperature and velocity, which are (17, 0.1), (17, 0.5), (21, 0.1), (21, 0.5)). Based on the four sampling locations, Kriging method was then applied to evaluate the response surface. The NSPSO algorithm was then performed to evaluate the distribution of optimal particles throughout the design space.

After the CFD simulations are finished, we generate the response surfaces using Kriging prediction. Then we run the NSPSO for 100 times and calculate the distribution density of optimal particles in design space. The distribution density contour is shown in Fig. 10(a) and the column charts in Figs. 10(b) and (c) indicate the projections of the density contour in temperature plane and velocity plane, respectively. As mentioned before, in order to make a comparison with the case described in Section 4.1, we want the sampling locations in this adaptive case would be a subset of the locations described in Fig. 6. It is easy to reach this goal by using halving method. Therefore, in Figs. 10(b) and (c), the red line in the middle cuts the plane into two sides and for each side, reserving or removing depends on the distribution density of the optimal solutions in the areas. For example, in Fig. 10(b), the right side (i.e. $T > 19$ °C) should be reserved for adding more sampling points rather than the left side (i.e. $T < 19$ °C), because there located much more optimal solutions (98%) on the right segment than the optimal solutions on the left segment (only 2%). Differently, in Fig. 10(c), both sides are required to add more sampling points, because the results show that there are almost as many optimal solutions on both sides (57% vs 43%). The promising area after first halving process has been determined which is shown in Fig. 12(a) (green shadow) and accordingly, the green points in Fig. 13 are inserted to be simulated in next iteration. The first iteration of process described in Fig. 9 has been finished. The next iteration process is almost same except with 4 more CFD sample data used in the Kriging prediction. The distribution density contour and having analysis are shown in Fig. 11. The acquired promising area in the second iteration process is indicated in Fig. 12(b) (red shadow) and the blue points in Fig. 13 are added, accordingly. Since the minimum sampling resolution has been reached, we stop adding more sampling points. Figure 13 illustrates the final CFD sampling locations.

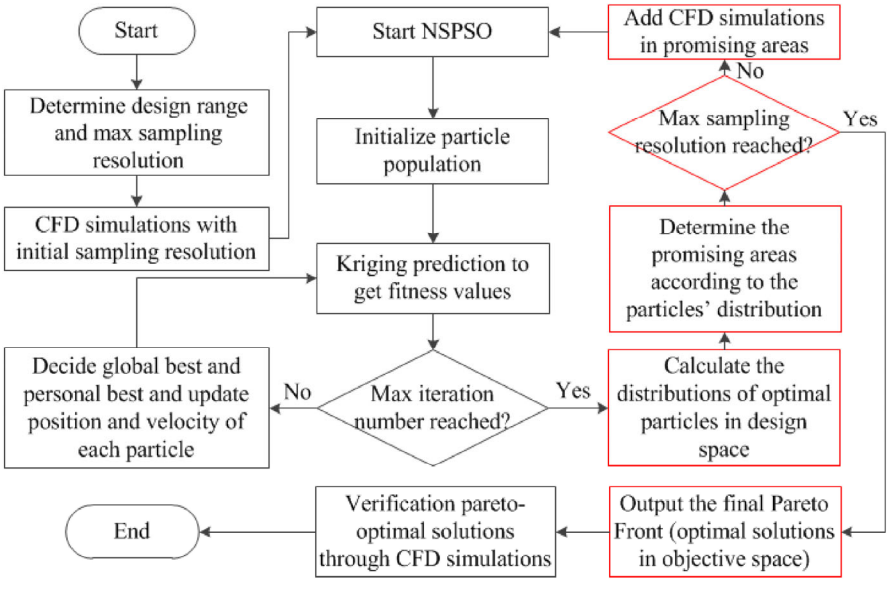

Fig. 9 Framework of the CFD-based multi-objective optimization approach with adaptive sampling procedure

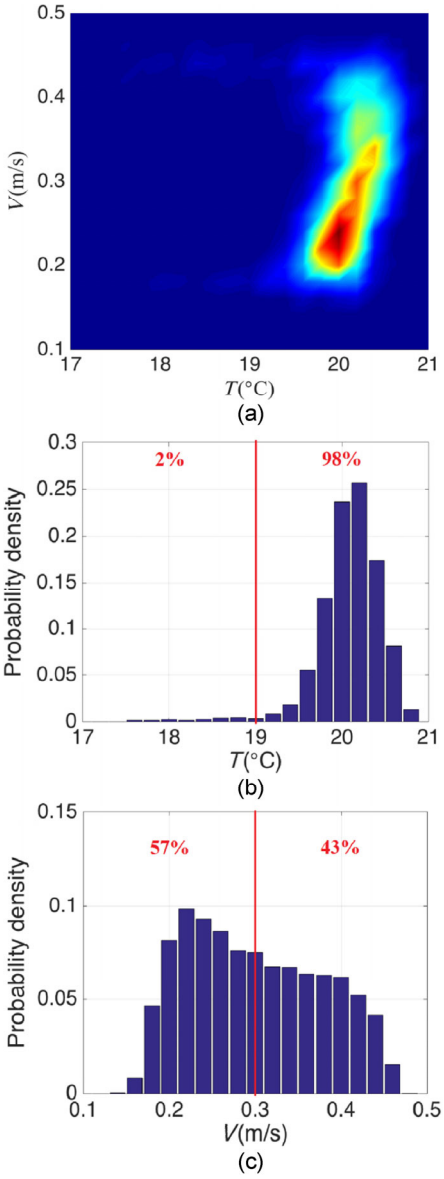

Fig. 10 Probability density of optimal solutions in the design space (initial 4 CFD sampling locations). (a) Contour of probability density in 2D design space. (b) Projected probability density on the temperature design space. (c) Projected probability density on the velocity design space

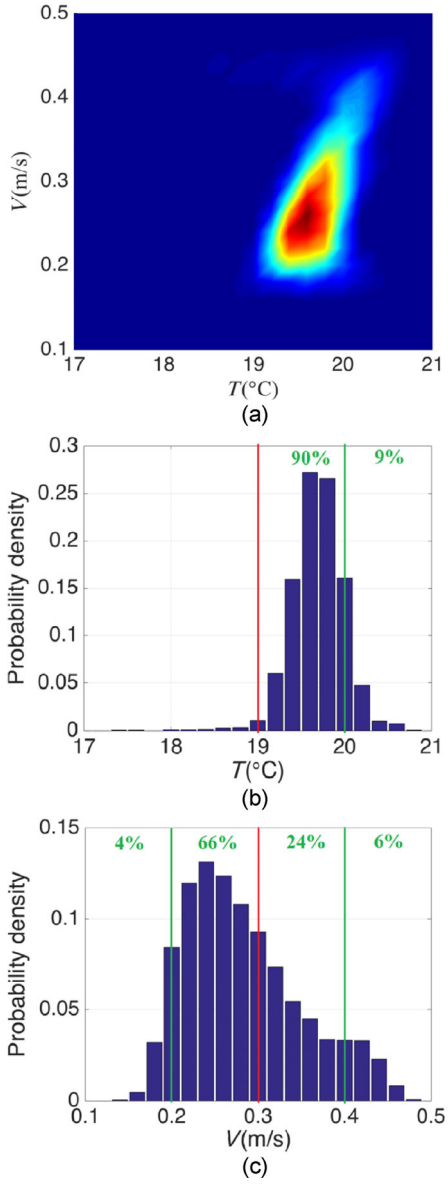

Fig. 11 Probability density of optimal solutions in design space (initial 4 CFD sampling locations + 4 new adding sampling locations). (a) Contour of probability density in 2D design space. (b) Projected probability density on the temperature design space. (c) Projected probability density on the velocity design space

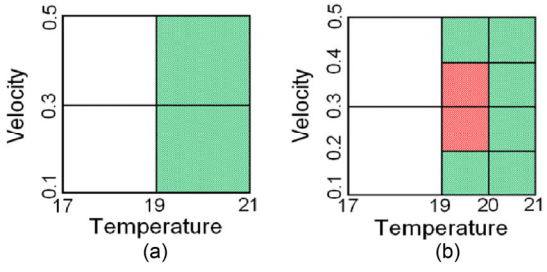

Fig. 12 Halving process in design space. (a) Halving process in first iteration of adaptive sampling procedure cutting the whole design space into 4 parts. (b) Halving process in second iteration of adaptive sampling procedure cutting the promising areas (green shaded in (a)) into 4 parts

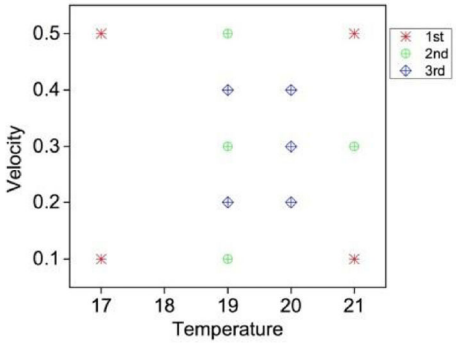

Fig. 13 Final CFD sampling locations in the adaptive sampling case

With the adaptive sampling procedure, one can notice that the final sample data only constructed with 13 sampling points. Therefore, only 13 CFD simulations were required in constructing the sample database. Table 3 shows a comparison of the required total computational time (i.e. the total of CFD simulation and the optimization computational time) for both cases. The table clearly shows that the adaptive sampling procedure could reduce up to 46.6% of the total computational time.

Although a significant saving has been achieved, it is essential to verify the accuracy of the optimal results with less sample data. Figure 14 shows the comparison of the predicted Pareto Front with the uniform sample data and the adaptive sampling procedure. As depicted, the blue dots are the solutions obtained from the uniform sample data; while solutions for adaptive sampling are represented in red dots. The figure clearly shows a good agreement of the Pareto Front obtained from both cases; demonstrating that the NSPSO algorithm together with the Kriging method are capable to maintain the accuracy of the optimal solution while achieving significant saving with less sample data.

A closer examination on the Kriging method in both cases is also presented here. Figure 15 shows the comparisons of the prediction design objectives (i.e. PMV, CO_2 concentrations and energy consumption) based on the uniform sampling data and the 13 sample data from adaptive sampling. As depicted, prediction differences between both cases are represented in the contour plot; while the probability distributions of the optimal solutions were also presented in while contour lines. As depicted, majority of difference

Table 3 Comparisons of CPU time consumptions (500 particles in the optimization process)

Approach	Procedure	CPU time (s)	Iterations	Total CPU time (s)
Traditional	CFD simulation	7.904E+04	25	1.976E+06
	Single objective PSO	1.168	~ 500	~ 5.840E+02
NSPSO + Kriging	CFD simulation	7.904E+04	13	1.028E+06
	NSPSO	1.372E+02	200	2.744E+04
Total saved CPU time		9.211E+05 (s) (**46.6%**)		

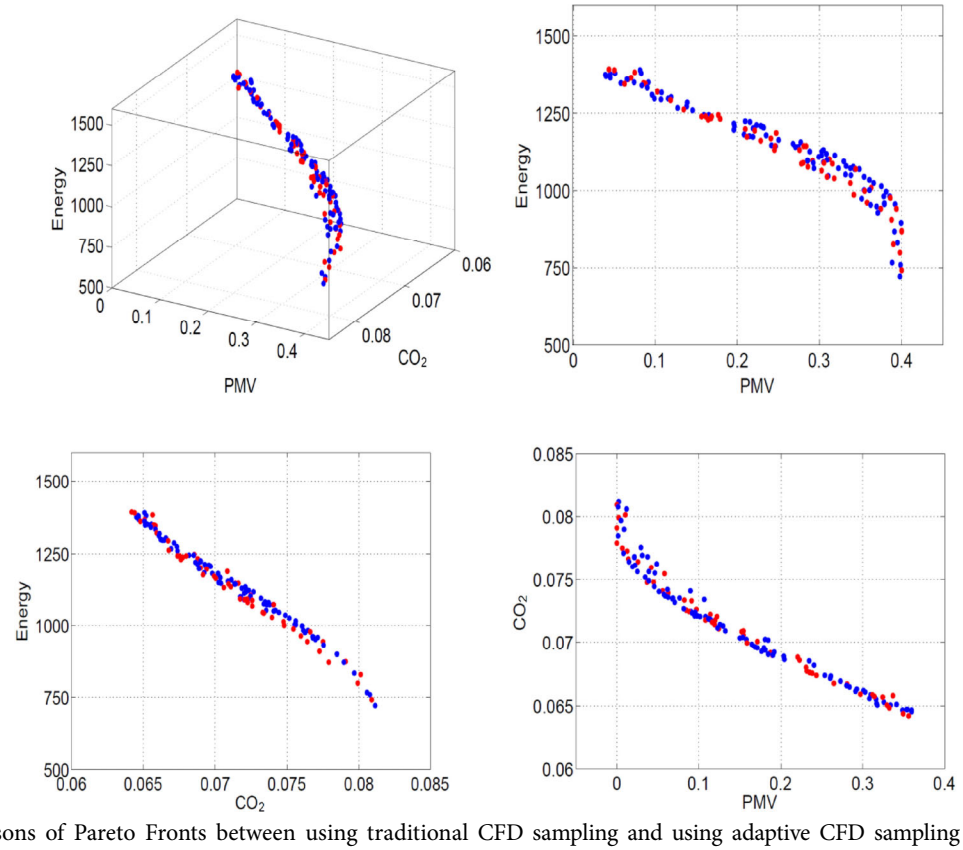

Fig. 14 Comparisons of Pareto Fronts between using traditional CFD sampling and using adaptive CFD sampling (blue—traditional, red—adaptive)

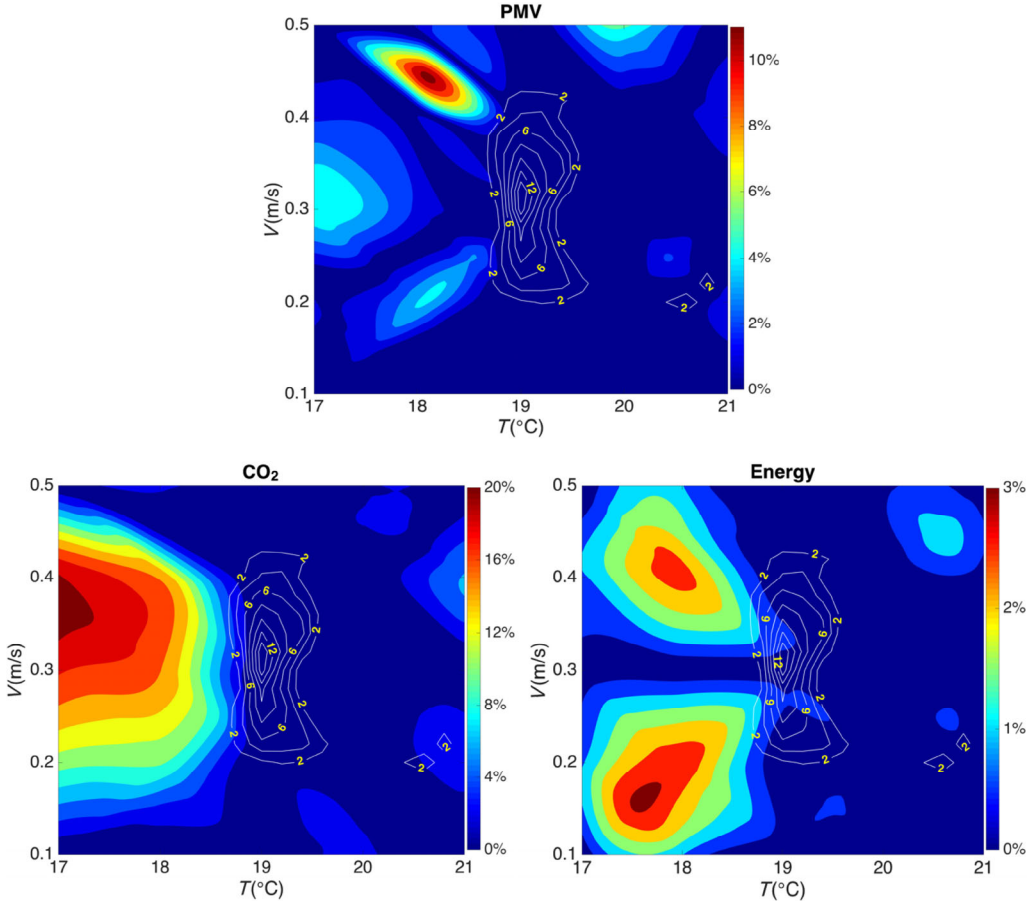

Fig. 15 Contours of Kriging prediction differences between using 13 CFD samples and 25 CFD samples (PMV, CO_2, energy, respectively)

between both cases are located on the left half of the design space where most of the sampling points were eliminated by adaptive sampling procedure. This clearly exemplifies that the adaptive sampling procedure has strategically allocated the sampling points where the optimal solutions are highly likely to be found. While relative error could be higher in other region, the lack of sampling data did not affect the accuracy of the final optimal solutions.

5 Conclusions

A multi-objective optimization platform has been proposed and developed by incorporating the nondominated sorting-based particle swarm optimization (NSPSO) algorithm with the Kriging method. To remedy the drawback of some previous studies, the NSPSO algorithm removes the necessity of using weighting factors in constructing the objective function and obtains the corresponding trade-off solutions (i.e. Pareto Front) for the given objective space. With the visualization of solutions in objective space, designers could easily pick up the most appropriate design solution according to their own judgments and preferences, rather than being struggled to decide the value of weighting factor in advance.

Special attention is also taken to minimize the computational cost where considerably large training sample based on computational fluid dynamics (CFD) simulations are usually required for the surrogate modelling. The Kriging method where the best linear unbiased value of the unobserved fields is estimated based on the known sampled data is adopted in the present study. One particular advantage of the Kriging method is its capability in achieving high prediction accuracy with relatively small training sample size. Predictions from the Kriging method are compared and assessed with the CFD predictions. The comparison has shown that the Kriging method provides excellent accuracy in prediction with the maximum error of 5.12%. In addition, with the proposed adaptive sampling procedure, further reduction of computational cost could be realized. Based on the given case study, the optimization platform achieves a saving of 46.6% of CPU time without sacrificing the accuracy of the optimal solution.

In this study, for assessing the performance of the proposed optimization algorithm, a benchmark case study that has been validated by many researchers (Yuan et al. 1999; Zhou and Haghighat 2009a,b; Li et al. 2013a,b) was selected. To further examine the capacity of the algorithm,

research work is currently carrying out to adopt and assess the proposed method with a more complex optimization case in related to the HVAC design of an airliner cabin occupied with passengers (Yan et al. 2014).

Acknowledgements

The financial support provided by an Australian Research Council grant (ARC Linkage LP130100236) is gratefully acknowledged.

References

Afrand M, Farahat S, Nezhad AH, Sheikhzadeh GA, Sarhaddi F, Wongwises S (2015). Multi-objective optimization of natural convection in a cylindrical annulus mold under magnetic field using particle swarm algorithm. *International Communications in Heat and Mass Transfer*, 60**:** 13–20.

Buratti C, Palladino D, Ricciardi P (2016). Application of a new 13-value thermal comfort scale to moderate environments. *Applied Energy*, 180**:** 859–866.

Buratti C, Ricciardi P (2009). Adaptive analysis of thermal comfort in university classrooms: correlation between experimental data and mathematical models. *Building and Environment*, 44**:** 674–687.

Buratti C, Ricciardi P, Vergoni M (2013). HVAC systems testing and check: A simplified model to predict thermal comfort conditions in moderate environments. *Applied Energy*, 104**:** 117–127.

Cardinale N, Stefanizzi P, Rospi G, Augenti V (2010). Thermal performance of a mobile home with light envelope. *Building Simulation*, 3**:** 331–338.

Carrese R, Sobester A, Winarto H, Li X (2011). Swarm heuristic for identifying preferred solutions in surrogate-based multi-objective engineering design. *AIAA Journal*, 49**:** 1437–1449.

Deb K (2001). Multi-objective Optimization Using Evolutionary Algorithms. Chichester, UK: John Wiley & Sons.

Deb K, Pratap A, Agarwal S, Meyarivan T (2002). A fast and elitist multiobjective genetic algorithm: NSGA-II. *IEEE Transactions on Evolutionary Computation*, 6**:** 182–197.

Fanger PO (1972). Thermal Comfort: Analysis and Applications in Environmental Engineering. New York: McGraw-Hill.

Forrester A, Sóbester A, Keane A (2008). Engineering Design via Surrogate Modelling: A Practical Guide. Chichester, UK: John Wiley & Sons.

Gangisetti K, Claridge DE, Srebric J, Paulus MT (2016). Influence of reduced VAV flow settings on indoor thermal comfort in an office space. *Building Simulation*, 9**:** 101–111.

Gano SE, Renaud JE, Martin JD, Simpson TW (2006). Update strategies for kriging models used in variable fidelity optimization. *Structural and Multidisciplinary Optimization*, 32**:** 287–298.

Gyulai L, Szabó S, De Kock DJ, Snyman JA (2007). A study of the feasibility of using mathematical optimisation to minimise the temperature in a smelter pot room. *Building and Environment*, 42**:** 2268–2278.

Hardwick J, Stout QF (2016). Adaptive Sampling Designs. University of Michigan. Available at http://web.eecs.umich.edu/~qstout/AdaptSample.html.

Hassan R, Cohanim B, De Weck O, Venter G (2005). A comparison of particle swarm optimization and the genetic algorithm. In: Proceedings of the 1st AIAA Multidisciplinary Design Optimization Specialist Conference, Austin, USA.

Hiyama K, Kato S, Ishida Y (2010). Thermal simulation: Response factor analysis using three-dimensional CFD in the simulation of air conditioning control. *Building Simulation*, 3**:** 195–203.

Journel AG, Huijbregts CJ (1978). Mining Geostatistics. London: Academic Press.

Kennedy J (2001). Swarm Intelligence. San Francisco: Morgan Kaufmann Publishers.

Kochetov N, Loktionov V, Sidorov A (2015). Using the Star CCM+ software system for modeling the thermal state and natural convection in the melt metal layer during severe accidents in VVER reactors. *Thermal Engineering*, 62**:** 663–672.

Krauss G, Kindangen J, Depecker P (1997). Using artificial neural networks to predict interior velocity coefficients. *Building and Environment*, 32**:** 295–303.

Laverge J, Janssens A (2013). Optimization of design flow rates and component sizing for residential ventilation. *Building and Environment*, 65**:** 81–89.

Li K, Su H, Chu J, Xu C (2013a). A fast-POD model for simulation and control of indoor thermal environment of buildings. *Building and Environment*, 60**:** 150–157.

Li K, Xue W, Xu C, Su H (2013b). Optimization of ventilation system operation in office environment using POD model reduction and genetic algorithm. *Energy and Buildings*, 67**:** 34–43.

Li X (2003). A non-dominated sorting particle swarm optimizer for multiobjective optimization. In: Proceedings of Genetic and Evolutionary Computation Conference, Chicago, USA, pp. 37–48.

He H-D, Lu W-Z, Xue Y (2014). Prediction of particulate matter at street level using artificial neural networks coupling with chaotic particle swarm optimization algorithm. *Building and Environment*, 78**:** 111–117.

Luh GC, Lin CY (2011). Optimal design of truss-structures using particle swarm optimization. *Computers and Structures*, 89**:** 2221–2232.

Martínez SZ (2013). Use of gradient-free mathematical programming techniques to improve the performance of multi-objective evolutionary algorithms. PhD Thesis, National Polytechnic Institute of Mexico, Mexico.

Nematchoua MK, Tchinda R, Ricciardi P, Djongyang N (2014). A field study on thermal comfort in naturally-ventilated buildings located in the equatorial climatic region of Cameroon. *Renewable and Sustainable Energy Reviews*, 39**:** 381–393.

Ravikumar P, Prakash D (2009). Analysis of thermal comfort in an office room by varying the dimensions of the windows on adjacent walls using CFD: A case study based on numerical simulation. *Building Simulation*, 2**:** 187–196.

Ricciardi P, Buratti C (2015). Thermal comfort in the Fraschini theatre (Pavia, Italy): Correlation between data from questionnaires, measurements, and mathematical model. *Energy and Buildings*, 99**:** 243–252.

Ricciardi P, Ziletti A, Buratti C (2016). Evaluation of thermal comfort in an historical Italian opera theatre by the calculation of the neutral comfort temperature. *Building and Environment*, 102**:** 116–127.

Stavrakakis GM, Karadimou DP, Zervas PL, Sarimveis H, Markatos NC (2011). Selection of window sizes for optimizing occupational comfort and hygiene based on computational fluid dynamics and neural networks. *Building and Environment*, 46**:** 298–314.

Tu J, Yeoh GH, Liu C (2008). Computational Fluid Dynamics: A Practical Approach. Burlington, MA, USA: Butterworth-Heinemann.

Varol Y, Avci E, Koca A, Oztop HF (2007). Prediction of flow fields and temperature distributions due to natural convection in a triangular enclosure using Adaptive-Network-Based Fuzzy Inference System (ANFIS) and Artificial Neural Network (ANN). *International Communications in Heat and Mass Transfer*, 34**:** 887–896.

Welle B, Haymaker J, Rogers Z (2011). ThermalOpt: A methodology for automated BIM-based multidisciplinary thermal simulation for use in optimization environments. *Building Simulation*, 4**:** 293–313.

Yan Y, Li X, Tu J (2014). Numerical study of passenger thermal effects on the transport characteristics of exhaled droplets in an airliner cabin. In: Proceedings of the 13th International Conference on Indoor Air Quality and Climate, Hong Kong, China.

Yuan X, Chen Q, Glicksman LR, Hu Y, Yang X (1999). Measurements and computations of room airflow with displacement ventilation. *ASHRAE Transactions*, 105(1): 340–350.

Zhai Z, Xue Y, Chen Q (2014). Inverse design methods for indoor ventilation systems using CFD-based multi-objective genetic algorithm. *Building Simulation*, 7**:** 661–669.

Zhao B (2009). Modeling pressure drop coefficient for cyclone separators: A support vector machine approach. *Chemical Engineering Science*, 64**:** 4131–4136.

Zhou L, Haghighat F (2009a). Optimization of ventilation system design and operation in office environment, Part I: Methodology. *Building and Environment*, 44**:** 651–656.

Zhou L, Haghighat F (2009b). Optimization of ventilation systems in office environment, Part II: Results and discussions. *Building and Environment*, 44**:** 657–665.